

Thermal boundary resistance predictions with non-equilibrium Green's function and molecular dynamics simulations

Yuanchen Chu,^{1,*} Jingjing Shi,^{2,*} Kai Miao,¹ Yang Zhong,² Prasad Sarangapani,¹ Tim Fisher,³ Gerhard Klimeck,^{1,4,5} Xiulin Ruan,² and Tillmann Kubis^{1,4,5,6}

¹*School of Electrical and Computer Engineering, Purdue University, West Lafayette, IN 47907, USA*

²*School of Mechanical Engineering, Purdue University, West Lafayette, IN 47907, USA*

³*Department of Mechanical and Aerospace Engineering, University of California, Los Angeles, CA 90095, USA*

⁴*Network for Computational Nanotechnology, Purdue University, West Lafayette, Indiana 47907, USA*

⁵*Purdue Center for Predictive Materials and Devices, West Lafayette, Indiana 47907, USA*

⁶*Purdue Institute of Inflammation, Immunology and Infectious Disease, West Lafayette, Indiana 47907, USA*

(Dated: 2 September 2019)

The non-equilibrium Green's function (NEGF) method with Büttiker probe scattering self-energies is assessed by comparing its predictions for the thermal boundary resistance with molecular dynamics (MD) simulations. For simplicity, the interface of Si/heavy-Si is considered, where heavy-Si differs from Si only in the mass value. With Büttiker probe scattering parameters tuned against MD in homogeneous Si, the NEGF-predicted thermal boundary resistance quantitatively agrees with MD for wide mass ratios. Artificial resistances that plagued NEGF calculations in homogeneous systems so far are absent in the present NEGF approach. Spectral transport information result from NEGF without transformations in its natural representation. The spectral results show that the scattering between different phonon modes plays a crucial role in thermal transport across interfaces.

Semiconductor nanodevices such as quantum cascade lasers, LEDs and thermoelectric devices are typically composed of several semiconductor materials¹⁻⁴. Scattering of thermal energy carriers at the interface between two materials results in thermal boundary resistance⁵. The size of the thermal boundary resistance was previously reported⁶ to be comparable to that of pure materials with lengths of a few to tens of nanometers. Predicting the thermal boundary resistance gives important insight into the device physics and enables design improvements. Often, molecular dynamics (MD) is used to model the thermal boundary resistance and reproduce experimental data⁷. Inelastic phonon scattering is included in MD simulations through the anharmonicity of the interatomic potential⁸. The non-equilibrium Green's function (NEGF) method⁹ is widely accepted as one of the most consistent methods for electronic quantum transport in nanodevices^{10,11}. In particular for predicting stationary device physics, NEGF is potentially more attractive than MD given that it is a spectral approach when setup in energy space. When electrons and phonons are both solved in the NEGF framework, interparticle interactions and energy and momentum transfer in e.g. self-heating or thermoelectric situations can be described on equal footing with the predictions of the respective particles' propagation¹². For phonon transport, however, the NEGF method has been used predominantly in the coherent (harmonic) regime due to the fact that the inclusion of incoherent scattering such as phonon-phonon decay usually requires solving polarization graphs in the self-consistent Born approximation which entails a large numerical load¹³. Coherent NEGF based on the Landauer approach has been plagued by artificial interface resistances in homogeneous systems⁶.

In this work, a numerically efficient method to solve phonon transport in the NEGF framework including phe-

nomenological phonon scattering with Büttiker probes is presented and benchmarked against MD. When solved for homogeneous systems, this NEGF method yields vanishing interface resistance. The thermal boundary resistance calculated with this NEGF method shows quantitative agreement with MD simulations. The extracted spectral transport information from NEGF shows that the different phonon modal contributions play an important role in thermal transport across the interface.

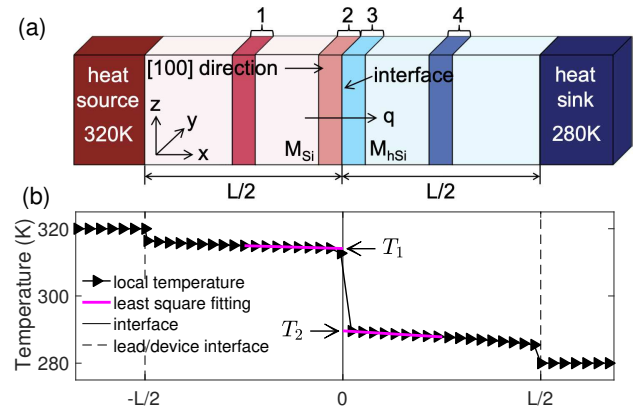


FIG. 1. (a) Simulation domain considered in this work. Regions marked by 1 through 4 are three atomic layers in the middle of Si, left to the interface, right to the interface and in the middle of heavy Si, respectively. (b) Schematic of the thermal boundary resistance extraction.

Figure 1(a) shows the simulation domain considered in both MD and NEGF. The system consists of Si to the left and heavy-Si to the right of an interface at position 0. The heavy-Si differs from Si only in its atomic mass ratio vs. Si $MR = M_{hSi}/M_{Si}$. For all simulations in this work, M_{Si} is fixed at 28.085u and a range of 1 to 10 is considered for MR . Transport is solved within a range $L/2$ to the left and right of the

*These authors contributed equally to this work, email: chu72@purdue.edu

interface. The lattice temperature for regions further to the left and right of the interface is assumed constant and to equal 320 K and 280 K, respectively. Phonon transport occurs along the x direction and the system is considered to be periodic along y and z directions. The harmonic phonon bandstructure is described with a Tersoff potential¹⁴ and the lattice constant is set to 5.431 Å. Details of the thermal boundary resistance extraction are illustrated in Fig. 1(b). Firstly, linear fits are performed on the local temperature profiles to the left and to the right of the interface, respectively. The local temperature T is obtained by minimizing the difference between the local phonon energy density and the product of a local Bose-Einstein distribution and the local phonon density of states¹⁵. Second, the temperatures T_1 and T_2 of the Si and heavy Si in the vicinity of the interface are determined with the fitted temperature profiles. Finally, the thermal boundary resistance is calculated as $R = (T_1 - T_2)/q$, where q is the simulated heat flux. Following the discussion in Ref. [16], three different device lengths L are simulated for each value of MR , and R is extracted for the limit of $1/L = 0$ by linear extrapolation.

The LAMMPS package¹⁷ is used for all MD simulations in this work. The lengths of both the heat source and the heat sink are $L/10$ and the simulation timestep is 0.4 fs. Periodic boundary conditions are applied in y and z directions while the fixed boundary condition¹⁸ is applied in the x direction. For MD calculations, the discretized device cross-section is of 8×8 conventional unit cells, with each conventional cell containing 8 atoms. First, a canonical ensemble (NVT) is considered and run for 1.2 ns to relax the structure, allowing the system to reach thermal equilibrium at 300 K. The system is then switched to a microcanonical ensemble (NVE) and a constant heat flux is added to the heat source and extracted from the heat sink for 12 ns. After the system reaches steady state, the local temperature of each cell is obtained by averaging over ten million timesteps in the last 4 ns. L of 92, 130 and 184 unit cells is used for MD based simulation of each MR value.

For all NEGF simulations, the nanodevice simulation tool NEMO5¹⁹ is used. Stationary Green's functions are solved in the energy domain, which gives spectral data without additional transformations. To calculate the harmonic interatomic force constants (IFCs), a $3 \times 3 \times 3$ unit cell bulk Si structure is relaxed in LAMMPS using the Tersoff potential¹⁴. The derivatives of the forces between atoms with respect to the atom position variations give the harmonic IFCs. These values are then loaded into NEMO5 to construct the dynamical matrix²⁰. Only the transport direction (x) is discretized in real space. The periodic directions (y and z) are represented with a single conventional unit cell. Longer-ranged periodicity is represented with the phonon momenta in reciprocal space. Anharmonic phonon decay is included via Büttiker probes²¹. The Büttiker probe self-energies at atom i with vibrational direction $m(x, y, z)$ are of the form

$$\Sigma_{BP(i,m)}^R(\omega) = -i \frac{2\omega\hbar^2}{\tau_{(i,m)}(\omega)}. \quad (1)$$

Following Ref. [22] we approximate the phonon frequency (ω) dependent scattering lifetime τ as isotropic and assume it

represents only the phonon-phonon Umklapp process¹⁵

$$\tau_{(i,m)}^{-1}(\omega) = \tau_i^{-1}(\omega) = BT_i\omega^2 e^{-C/T_i}. \quad (2)$$

$T_{(i)}$ is the phonon Büttiker probe temperature of the atom i . Since the phonon Green's functions are solved with the recursive Green's function (RGF) method²², the device is partitioned into slabs perpendicular to transport direction. This limits the peak memory usage during computation, but requires the Büttiker probe self-energies to be equal throughout each slab. The parameters B (5×10^{-20} s/K) and C (430 K) are chosen such that the NEGF prediction of the bulk Si thermal conductivity agrees with the MD solution (see Fig. 2(a)). L of 146, 184 and 220 unit cells is used for NEGF based simulation of each MR value.

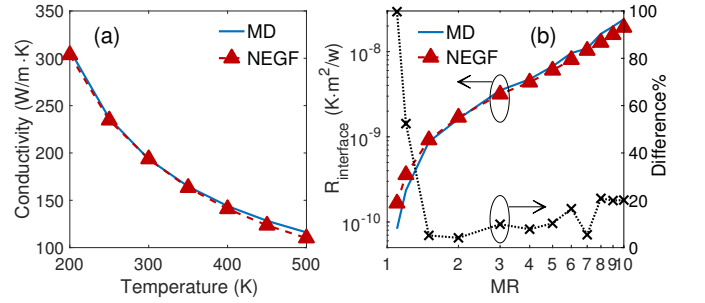


FIG. 2. (a) Thermal conductivity of bulk Si calculated with MD and NEGF. The Büttiker probe parameters B and C are fitted such that the transport results of NEGF agree with MD. (b) Thermal boundary resistance as a function of the mass ratio (MR) calculated by MD and NEGF with the fitted parameters B and C of (a). The dashed line is the relative difference of the two methods and is defined as $(NEGF - NEMD)/NEMD \times 100\%$.

The spatial distribution of local phonon density of states (LDOS) can illustrate the contributions of different phonon modes to the heat flux in various regions. For this purpose, four regions of interest, consisting of three atomic layers each are defined in Fig. 1(a). The LDOS $\phi_i(\omega)$ of any region i of these regions is averaged over all of its atoms. For a given phonon frequency, the L1-norm of the LDOS summed over all regions is defined as

$$\|\phi_{tot}(\omega)\| = \sum_{i=1}^4 \phi_i(\omega). \quad (3)$$

The relative contribution of LDOS of region i is then defined as

$$R_i(\omega) = \frac{\phi_i(\omega)}{\|\phi_{tot}(\omega)\|}. \quad (4)$$

Figure 2(b) shows the thermal boundary resistance as a function of MR calculated with NEGF agrees quantitatively with the MD predictions. For both methods, the thermal boundary resistance increases exponentially with MR and vanishes when MR tends to unity (i.e. for a homogeneous system). Small remaining difference between the MD and NEGF results are systemic to the different treatment of phonon

modes perpendicular to the transport direction: In NEGF, the phonon momentum perpendicular to transport is explicitly resolved as a parameter in the Dyson and Keldysh equations²². In contrast, MD calculations require as large as possible unit cells perpendicular to transport to cover as many phonon modes with long wave lengths in these directions as feasible. Another source of differences can be the open boundary condition in transport direction: Figures 3 (a) and (b) benchmark the open boundary condition treatment in MD and NEGF, since they illustrate finite-size effects⁷ with the thermal boundary resistance R as a function of the inverse system length $1/L$. For MD, the slope of R vs $1/L$ increases with the mass ratio MR , i.e. with reducing average sound velocity in the device. This agrees with similar findings discussed in detail in Ref. [7]. In contrast to the finite sized boundary reservoirs of MD, contact self-energies in NEGF incorporate semi-infinite leads as charge reservoirs²³. Accordingly, we observe the slope of R vs. $1/L$ in NEGF predictions is much smaller than that of MD. Also its increase with MR is comparably negligible. This different boundary treatment is another source of some differences between MD and NEGF seen in Fig. 2 (b).

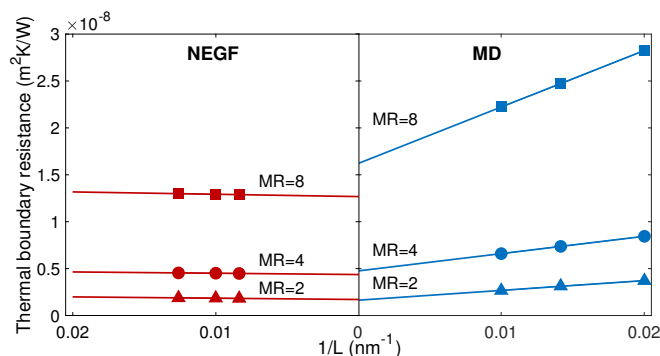


FIG. 3. Linear extrapolation of NEGF and MD for three MR values. MD results show a stronger dependence on the length of the device. Open boundary conditions included in NEGF with contact self-energies give almost device size independent results.

Figure 4(a) shows the phonon density of states (DOS) in homogeneous Si and heavy-Si solved with NEGF. The DOS of heavy-Si is limited to energies at or below 33.3 meV, two times less than in native Si in agreement with the applied $MR = 4$. Incoherent phonon scattering allows phonons with energies above this heavy-Si cutoff energy to propagate. This is illustrated in Figs. 4(b), (c) and (d) with the energy resolved current densities of the heat source and heat sink of the device in Fig. 1(a) when solved in NEGF with different scattering strengths. In Fig. 4(b), normal scattering strength (fitted to reproduce the MD-calculated bulk thermal conductivity) is applied. The source current with energies above the energy cutoff is finite since its corresponding phonons can relax to lower energies at the heavy-Si side via inelastic scattering. In Fig. 4(c), an artificially weak scattering strength is used ($1/20\times$ normal scattering strength). Accordingly, the profiles of current in both the heat source and sink follow the profile of the heavy-Si DOS. In contrast, Fig. 4(d) shows the NEGF

results when artificially strong scattering is used ($20\times$ normal scattering strength). The current profiles in the heat source and heat sink follow the profiles of the DOS in the Si and the heavy-Si leads, respectively. The results show that stronger inelastic scattering brings the system closer to local thermodynamic equilibrium.

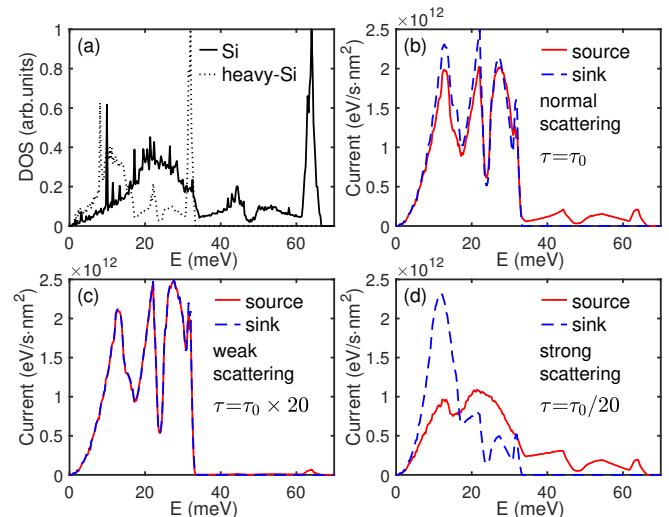


FIG. 4. (a) Energy resolved (transverse momentum integrated) density of states in Si and heavy-Si leads. (b)~(d) Energy resolved (transverse momentum integrated) current of NEGF in the heat source and sink calculated with normal, artificially weak ($1/20\times$) and artificially strong ($20\times$) scattering strengths, respectively.

In Fig. 4(b), four current peaks in the heavy-Si heat sink are located at 12 meV, 22 meV, 27 meV and 32 meV, respectively. They correspond to the four peaks of the heavy-Si DOS shown in Fig. 4(a). The relative magnitudes of the four current peaks do not follow the relative magnitudes of the four DOS peaks (i.e., the list of current peaks arranged in decreasing order of magnitude is 22 meV > 12 meV > 27 meV > 32 meV, whereas the same list according to the DOS magnitude is 32 meV > 12 meV > 22 meV > 27 meV). Without interfaces involved, the current is expected to be proportional to the product of the DOS and the group velocity²⁴. The results of Figs. 4 can be understood in Fig. 5, since it illustrates the different relative contributions of phonon modes in different device areas. Phonon modes around 12 meV reside nearly exclusively in the heavy-Si. Consequently, they contribute less to the overall heat current. In contrast, phonon modes around 22 meV are present in all 4 device regions considered in Fig. 5. Therefore, these modes can maintain a higher contribution to the total heat current.

In conclusion, NEGF with Büttiker probe scattering is applied to the thermal boundary resistance of the Si/heavy-Si interface. The empirical NEGF scattering parameters are tuned to reproduce the thermal conductivity of homogeneous Si predicted by MD. The scattering parameters proved to be transferable, since the NEGF results of the thermal boundary resistance quantitatively agrees with MD results for mass ratios ranging from 1 to 10. Finite interface resistances in homogeneous structures that have plagued previous NEGF

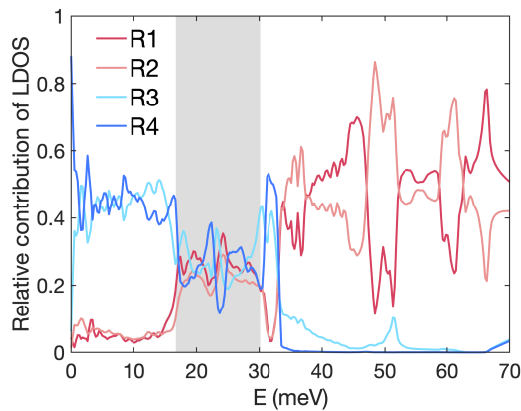


FIG. 5. The ratio of the phonon mode in regions 1 ~ 4 defined in Fig. 1 and by Eq. 4 ($\sum_{i=1}^4 R_i = 1$). The evenly distributed phonon modes around 22 meV (marked by the gray area) result in the highest current peak at 22 meV (see Fig. 4(b)) although having a lower DOS and lower group velocity compared to those at 12 meV.

phonon transport implementations⁶ is absent in the presented approach. Besides, the present NEGF approach is found to be numerically more efficient than MD. Thanks to the open boundary conditions, NEGF shows virtually no finite-size effects compared to MD. The analysis of the NEGF spectral information shows that the scattering between different phonon modes determines the phonon energy current flow across interfaces.

¹Z. I. Alferov, “The history and future of semiconductor heterostructures,” *Semiconductors* **32**, 1–14 (1998), arXiv:arXiv:1011.1669v3.

²J. Faist, F. Capasso, D. L. Sivco, C. Sirtori, L. Albert, T. Hall, J. Faist, F. Capasso, D. L. Sivco, C. Sirtori, A. L. Hutchinson, and A. Y. Cho, “Quantum Cascade Laser Hutchinson and Alfred Y. Cho Published by : American Association for the Advancement of Science Stable URL : <http://www.jstor.org/stable/2883703> JSTOR is a not-for-profit service that helps scholars, researchers, and students disc,” **264**, 553–556 (1994).

³S. Nakamura, T. Mukai, and M. Senoh, “Candela-class high-brightness InGaN/AlGaIn double-heterostructure blue-light-emitting diodes,” *Applied Physics Letters* **64**, 1687–1689 (1994), arXiv:arXiv:1011.1669v3.

⁴M. L. Tsai, S. H. Su, J. K. Chang, D. S. Tsai, C. H. Chen, C. I. Wu, L. J. Li, L. J. Chen, and J. H. He, “Monolayer MoS₂heterojunction solar cells,” *ACS Nano* **8**, 8317–8322 (2014), arXiv:arXiv:1408.1149.

⁵E. T. Swartz and R. O. Pohl, “Thermal boundary resistance,” *Reviews of Modern Physics* **61**, 605–668 (1989).

⁶E. S. Landry and A. J. H. McGaughey, “Thermal boundary resistance predictions from molecular dynamics simulations and theoretical calculations,” *Physical Review B - Condensed Matter and Materials Physics* **80**, 1–11 (2009).

- ⁷P. K. Schelling, S. R. Phillpot, and P. Keblinski, “Comparison of atomic-level simulation methods for computing thermal conductivity,” *Physical Review B* **65**, 1–12 (2002).
- ⁸P. E. Hopkins, “Multiple phonon processes contributing to inelastic scattering during thermal boundary conductance at solid interfaces,” *Journal of Applied Physics* **106** (2009), 10.1063/1.3169515.
- ⁹S. Datta, “Nanoscale device modeling: the Green’s function method,” *Superlattices and Microstructures* **28**, 253–278 (2000).
- ¹⁰J. Knoch, S. Mantl, and J. Appenzeller, “Impact of the dimensionality on the performance of tunneling fets: Bulk versus one-dimensional devices,” *Solid-State Electronics* **51**, 572–578 (2007), special Issue: Papers selected from the 2006 ULIS Conference.
- ¹¹A. Mátyás, T. Kubis, P. Lugli, and C. Jirasschek, “Comparison between semiclassical and full quantum transport analysis of THz quantum cascade lasers,” *Physica E: Low-Dimensional Systems and Nanostructures* **42**, 2628–2631 (2010).
- ¹²C. Stieger, A. Szabo, and M. Luisier, “Ab-initio quantum transport simulation of self-heating in single-layer 2-D materials Ab-initio quantum transport simulation of self-heating in single-layer 2-D materials,” **045708** (2017), 10.1063/1.4990384.
- ¹³M. Luisier, “Atomistic modeling of anharmonic phonon-phonon scattering in nanowires,” *Phys. Rev. B* **86**, 245407 (2012).
- ¹⁴J. Tersoff, “Modeling solid-state chemistry: Interatomic potentials for multicomponent systems,” *Phys. Rev. B* **39**, 5566–5568 (1989).
- ¹⁵K. Miao, S. Sadasivam, J. Charles, G. Klimeck, T. S. Fisher, and T. Kubis, “Büttiker probes for dissipative phonon quantum transport in semiconductor nanostructures,” *Applied Physics Letters* **108** (2016), 10.1063/1.4944329.
- ¹⁶D. Sellan, E. Landry, J. Turney, a. McGaughey, and C. Amon, “Size effects in molecular dynamics thermal conductivity predictions,” *Physical Review B* **81**, 1–10 (2010).
- ¹⁷S. Plimpton, “Fast parallel algorithms for short-range molecular dynamics,” (1995), arXiv:nag.2347 [10.1002].
- ¹⁸B. J. Alder and T. E. Wainwright, “Studies in molecular dynamics. i. general method,” *The Journal of Chemical Physics* **31**, 459–466 (1959), <https://doi.org/10.1063/1.1730376>.
- ¹⁹S. Steiger, M. Povolotskyi, H. H. Park, T. Kubis, and G. Klimeck, “Nemo5: A parallel multiscale nanoelectronics modeling tool,” *IEEE Transactions on Nanotechnology* **10**, 1464–1474 (2011).
- ²⁰A. Paul, M. Luisier, and G. Klimeck, *Journal of Computational Electronics*, Vol. 9 (2010) pp. 160–172, arXiv:1009.6188.
- ²¹M. Büttiker, “Four-terminal phase-coherent conductance,” *Phys. Rev. Lett.* **57**, 1761–1764 (1986).
- ²²S. Sadasivam, N. Ye, J. P. Feser, J. Charles, K. Miao, T. Kubis, and T. S. Fisher, “Thermal transport across metal silicide-silicon interfaces : First-principles calculations and Green ’ s function transport simulations,” **085310**, 1–15 (2017).
- ²³S. Datta, *Quantum Transport: Atom to Transistor* (Cambridge University Press, 2005).
- ²⁴S. Datta, *Electronic Transport in Mesoscopic Systems*, Cambridge Studies in Semiconductor Physics and Microelectronic Engineering (Cambridge University Press, 1995).